

Article

Mixed Valanced V^{3+} , V^{2+} Phosphate $Na_7V_4(PO_4)_6$: A Structural Analogue of Mineral Yurmarinite

Galina Kiriukhina ^{1,2,*} , Valentina Nesterova ¹, Olga Yakubovich ^{1,*} , Anatoly Volkov ¹, Olga Dimitrova ¹, Alexander Trigub ³ and Konstantin Lyssenko ¹ 

¹ M.V. Lomonosov Moscow State University, Leninskiye Gory 1, Moscow 119991, Russia

² The Institute of Experimental Mineralogy RAS, Akademika Osip'yana st. 4, Chernogolovka 142432, Russia

³ National Research Centre "Kurchatov Institute", Akademika Kurchatova pl. 1, Moscow 123182, Russia

* Correspondence: g-biralo@yandex.ru (G.K.); yakubol@geol.msu.ru (O.Y.)

Abstract: Two sodium vanadium phosphates, synthetic analogues of the minerals kosnarite, $Na_3V_2(PO_4)_3$, and yurmarinite, $Na_7V_4(PO_4)_6$, were obtained by hydrothermal synthesis simulating a natural hydrothermal solution. While the $Na_3V_2(PO_4)_3$ phase belongs to the NASICON family and is well-known for its high-ionic conductivity, the new $Na_7V_4(PO_4)_6$ compound is a rare case of V^{2+} -containing oxosalts, which are hard to prepare due to their instability in air. Here we report the crystal structure of heterovalent vanadium phosphate studied by single crystal X-ray diffraction, XANES spectroscopy, and topological ion migration modelling. A discussion of divalent vanadium compounds of both natural and synthetic origin is also given, with a review of the methods for their synthesis and a comparative analysis of V–O bond lengths.

Keywords: crystal structure; yurmarinite; divalent vanadium; hydrothermal synthesis; X-ray diffraction; XANES spectroscopy



Citation: Kiriukhina, G.; Nesterova, V.; Yakubovich, O.; Volkov, A.; Dimitrova, O.; Trigub, A.; Lyssenko, K. Mixed Valanced V^{3+} , V^{2+} Phosphate $Na_7V_4(PO_4)_6$: A Structural Analogue of Mineral Yurmarinite. *Minerals* **2022**, *12*, 1517. <https://doi.org/10.3390/min12121517>

Academic Editors: Tamara Đorđević, Natalia V. Zubkova and Igor Djerdj

Received: 1 November 2022

Accepted: 24 November 2022

Published: 27 November 2022

Publisher's Note: MDPI stays neutral with regard to jurisdictional claims in published maps and institutional affiliations.



Copyright: © 2022 by the authors. Licensee MDPI, Basel, Switzerland. This article is an open access article distributed under the terms and conditions of the Creative Commons Attribution (CC BY) license (<https://creativecommons.org/licenses/by/4.0/>).

1. Introduction

Due to its high chemical activity, variable valence, and ability to form different stable complexes, vanadium is an essential element of more than 200 minerals. V^{3+} -containing minerals are mostly igneous silicates, V^{5+} in the form of $[VO_4]^{3-}$ anion occurs mainly as hydrothermal vanadates, and V^{4+} as the $(VO)^{2+}$ cation forms minerals of mixed origin, such as metamorphic, hydrothermal or weathering [1]. The genesis of V natural phases correlates with the oxidation state of vanadium, which directly depends on the pH value of the crystallization medium and the reduction potential [2]. While V^{3+} is generally stable under highly anoxic conditions, V^{4+} is present in moderately reducing environments, particularly under acidic conditions, and V^{5+} is stable under oxygen conditions and in sub-oxygen alkaline environments [3]. Accordingly, only the III, IV, and V valence states of vanadium are relevant under conditions typical for the earth's surface.

Conversely, divalent vanadium is unstable in the air and rarely forms natural phases. The unique V^{2+} -bearing mineral dellagiustaite, $Al(V^{2+}, V^{3+})_2O_4$, was recently found in rocks from Sierra de Comechingones, San Luis, Argentina, and in late pyroclastic ejecta of small Cretaceous basalt volcanoes exposed at Mt Carmel, Northern Israel [4]. It crystallizes in the inverse spinel structure type and cannot be labeled as "vanadium coulsonite" because of the predominance of Al over V^{3+} in the tetrahedral position. Dellagiustaite is associated with hibonite, $CaAl_{12}O_{19}$, and grossite, $CaAl_4O_7$, which constitute the modal composition of the rock. At the same time, V and Al metal alloys indicate significantly reducing conditions in the assemblages from both localities. The authors propose that mineral formation results from the interaction of deep-seated magmas and $CH_4 \pm H_2$ fluids in volcanic feeder systems [4].

We obtained a new sodium phosphate, $Na_7V_4(PO_4)_6$, with V atoms in the 2+ and 3+ oxidation states under hydrothermal conditions. It was synthesized together with the

NASICON-type $\text{Na}_3\text{V}_2(\text{PO}_4)_3$. The new compound is isostructural to the fumarole mineral yurmarinite, $\text{Na}_7(\text{Fe}^{3+}, \text{Mg}, \text{Cu})_4(\text{AsO}_4)_6$ [5]. Presumably, yurmarinite was formed under strongly oxidizing conditions of the Arsenatnaya fumarole in association with several alluaudite-type arsenates, namely hatertite, $\text{Na}_2(\text{Ca}, \text{Na})(\text{Fe}^{3+}, \text{Cu})_2(\text{AsO}_4)_3$, bradaczekite, $\text{NaCu}_4(\text{AsO}_4)_3$, and johillerite, $\text{NaMg}_3\text{Cu}(\text{AsO}_4)_3$. The high volatility of O in fumarolic gases causes high-valency states of As^{5+} and Fe^{3+} in all phases [5]. In octahedral positions of yurmarinite crystal structure, Mg^{2+} and Cu^{2+} cations isomorphically substitute Fe^{3+} . Moreover, the yurmarinite structure-type unites synthetic phosphates [6], arsenates [7–9], and even molybdates [10] with the general formula $(X)_6(M1)(M2)(M3)_3(\text{TO}_4)_6$ [11]. Most of them contain Na in the X and M1 positions but Fe^{2+} and Fe^{3+} inside the M2 and M3 octahedra. The preparation of heterovalent iron compounds is standard. However, the oxosalts containing V^{2+} are exotic because of their complicated synthesis and low stability. As part of our program of studying mineralogically probable V-bearing phases [12–15], we present here the results of hydrothermal synthesis, crystal structure, and comparative crystal chemistry of a new sodium and vanadium (II, III) orthophosphate $\text{Na}_7\text{V}_4(\text{PO}_4)_6$.

2. Materials and Methods

2.1. Hydrothermal Synthesis and Scanning Electron Microscopy

High-temperature hydrothermal synthesis was carried out in a phosphate system with sodium and vanadium cations. Chemically pure primary reagents V_2O_3 2 g (13.3 mmol) and NaCl 2 g (34.2 mmol) were ground and mixed as powders in the presence of a small amount of 0.3 g $\text{Na}_3\text{C}_6\text{H}_5\text{O}_7$ (1.2 mmol) taken as redox agent. All components were dissolved in 7 mL of 1M aqueous solutions of H_3PO_4 and placed in a copper-lined nickel–chromium alloy autoclave of 14 mL capacity. The synthesis was performed at a temperature of 723 K and a pressure of 50 MPa. The synthesis duration was 20 days, sufficient to complete the crystallization reactions. The product was cooled to room temperature for over 24 h and washed with hot distilled water. As a result, well-faceted crystals of two phases were obtained: black flattened crystals with rhombohedral habitus and a vitreous luster (Figure 1) and yellow crystals of cubic shape with a strong luster.

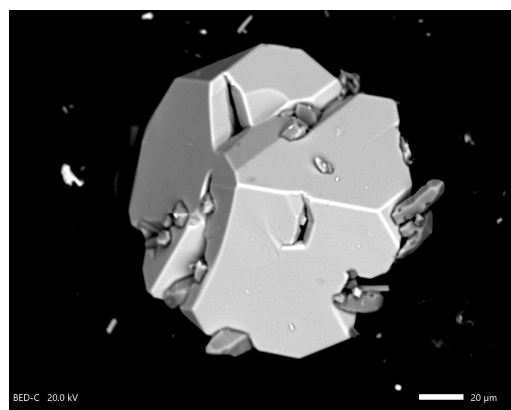


Figure 1. SEM image of the $\text{Na}_7\text{V}_4(\text{PO}_4)_6$ crystal with rhombohedral and prismatic faceting.

X-ray microprobe spectral analysis was performed at a Jeol JSM-6480LV SEM with an energy-dispersive spectrometer Oxford X-Man^N (Laboratory of Analytical Techniques of High Spatial Resolution, Dept. of Petrology, Moscow State University, Russia). EDS analysis revealed that both crystalline phases include V, Na, P, and O atoms. After a preliminary X-ray experiment, yellow isometric crystals were identified as $\text{Na}_3\text{V}_2(\text{PO}_4)_3$ with the NASICON structure type [16]. The second black phase of the rhombohedral habitus was diagnosed as a new compound and became the subject of X-ray diffraction analysis and crystal–chemical discussion.

2.2. X-ray Diffraction and X-ray Absorption Spectroscopy

Low-temperature ($T = 110$ K) X-ray diffraction experimental data were collected on a Bruker D 8 Quest single-crystal X-ray diffractometer, (Bruker Corporation, Billerica, MA, USA) (MoK α radiation). The dataset was corrected for background, Lorentz and polarization effects, and absorption. All calculations were performed within the WinGX program system, Version 2021.3 [17]. The trigonal crystal structure of the new phase was solved by direct methods in the rhombohedral space group $R\bar{3}c$ and refined in the anisotropic approximation of thermal vibrations of atoms with the SHELX programs (SHELXS 2014/6 [18], SHELXL 2018/3 [19]) using the F^2 data to residuals $R = 0.023$ and $S = 1.04$. As a result of the refinement, the crystal–chemical formula of the new compound was established to be $\text{Na}_7\text{V}_4[\text{PO}_4]_6$. The results of semiquantitative EDS analysis support it. Furthermore, the formula’s electroneutrality may be achieved by supposing a mixed population of two octahedral structural sites by V^{3+} and V^{2+} ions. Therefore, the compound presents a rare case of $\text{V}^{2+}/\text{V}^{3+}$ heterovalent phosphate with the crystal–chemical formula $\text{Na}_7(\text{V}^{3+}_{0.75}\text{V}^{2+}_{0.25})(\text{V}^{3+}_{0.75}\text{V}^{2+}_{0.25})_3[\text{PO}_4]_6$. The simplified formula $\text{Na}_7\text{V}^{3+}_3\text{V}^{2+}[\text{PO}_4]_6$ clearly shows three times more V^{3+} than V^{2+} ions. The range of V–O distances, bond valence calculation, and XANES spectroscopy confirm it. In Table 1, we report the crystallographic characteristics of the phase, the experimental conditions of data collection, and the results of crystal structure refinement. Table S1 lists the atomic coordinates and equivalent anisotropic displacement parameters. Figure S1 shows the calculated pattern for $\text{Na}_7\text{V}_4[\text{PO}_4]_6$. Characteristic distances are given in Table 2. We deposited structural data via the joint CCDC/FIZ Karlsruhe deposition service as CSD 2214946. It can be obtained free of charge from FIZ Karlsruhe via www.ccdc.cam.ac.uk/structures accessed on 24 October 2022.

Table 1. Experimental details for $\text{Na}_7\text{V}_4(\text{PO}_4)_6$.

Crystal Data	
Chemical formula	$\text{Na}_7\text{V}_4\text{P}_6\text{O}_{24}$
M_r	934.51
Crystal system, space group	Trigonal, $R\bar{3}c:H$
Temperature (K)	110
a, c (\AA)	13.3463 (19), 17.809 (4)
V (\AA^3)	2747.2 (10)
Z	6
Radiation type	Mo K α
μ (mm^{-1})	2.81
Crystal size (mm)	$0.08 \times 0.08 \times 0.04$
Data Collection ¹	
Diffractometer	Bruker D8 Quest
Absorption correction	Multi-scan
T_{\min}, T_{\max}	0.453, 0.494
No. of measured, independent and observed [$I > 2\sigma(I)$] reflections	9263, 894, 781
R_{int}	0.045
$(\sin \theta / \lambda)_{\text{max}}$ (\AA^{-1})	0.703
Refinement	
$R[F^2 > 2\sigma(F^2)], wR(F^2), S$	0.023, 0.059, 1.04
No. of reflections	894
No. of parameters	65
$\Delta\rho_{\text{max}}, \Delta\rho_{\text{min}}$ (e \AA^{-3})	0.46, -0.49

¹ Computer programs: *CrysAlis PRO* [20], *SADABS* 2016/2 [21], *Diamond* [22].

Table 2. Selected distances (Å).

V1 Octahedron		Na1 Octahedron	
V ₁ —O ₃ × 6	2.0173 (13)	Na ₁ —O ₄ × 6	2.3653 (14)
V2 Octahedron		Na2 [6+3] Polyhedron	
V ₂ —O ₁ × 2	1.9878 (13)	Na ₂ —O ₄	2.2706 (16)
V ₂ —O ₂ × 2	1.9942 (14)	Na ₂ —O ₁	2.5290 (16)
V ₂ —O ₃ × 2	2.0548 (13)	Na ₂ —O ₄	2.5718 (17)
		Na ₂ —O ₂	2.5721 (16)
P Tetrahedron		Na ₂ —O ₄	2.6202 (17)
P—O ₄	1.5103 (14)	Na ₂ —O ₂	2.6401 (17)
P—O ₂	1.5428 (15)	Na ₂ —O ₁	2.8084 (17)
P—O ₁	1.5513 (14)	Na ₂ —O ₃	2.8765 (16)
P—O ₃	1.5676 (14)	Na ₂ —O ₁	3.0213 (14)

To confirm the presence of V²⁺ in the compound, we studied X-ray absorption near-edge structure (XANES) at the K-edge of vanadium (obtained at the Structural Materials Science beamline [23] of the Kurchatov Synchrotron Radiation Source, Moscow, Russia). The parameters of the experiment were the following. The electron beam's energy of X-ray synchrotron radiation was 2.5 GeV at an average current of 60–100 mA. The absorption spectra were collected in the fluorescent radiation detection mode, i.e., the X-ray intensity was measured up to the sample, and the fluorescent radiation was detected. An ionization chamber was used to measure the X-ray beam intensity. The fluorescent radiation was captured with the help of an Amptek SDD detector. X-ray absorption spectra were processed by standard procedures for background extraction and normalized to the magnitude of the absorption jump. This procedure was performed using the Larch software package [24].

3. Results

3.1. Crystal Structure Description in terms of Close-Packing

The crystal structure of Na₇V₄(PO₄)₆ is based on the main structural units shown in Figure 2a. They are two symmetrically independent vanadium octahedra and an orthophosphate tetrahedron. The PO₄ polyhedron has minimal C₁ symmetry and represents a distorted trigonal pyramid. Three oxygen atoms O₁–O₃ are located at distances of 1.543(1)–1.568(1) Å from the P atom (Table 2). They lie in a plane approximately parallel to (001). Additionally, they are involved in the coordination of vanadium cations (Figure 2b). The fourth oxygen vertex O₄ at a shortened P–O₄ distance of 1.510(1) Å points almost perpendicular to the base of the phosphate tetrahedron along the *c*-axis (Figures 2 and 3). In addition to phosphorus, the O₄ atom coordinates sodium cations. V atoms occupy two positions in the structure with site symmetry 32 and 2. In an octahedron with D₃ symmetry, all V₁–O₃ bond lengths are equivalent and equal to 2.017(1) Å; in the octahedron with lower C₂ symmetry, the V–O bond lengths vary from 1.988(1) to 2.055(1) Å (Table 2). The average V–O distances in both polyhedra are close and equal to 2.017 and 2.012 Å, respectively.

In the crystal structure of Na₇V₄(PO₄)₆, vanadium polyhedra unite in the cluster, in which every V₁O₆ octahedron on a three-fold axis shares common edges with three surrounding V₂O₆ octahedra (Figures 2b and 3a). These clusters do not link with each other along the [001] direction. Instead, they form the close-packed layers parallel to the (001) plane and alternate along the *c*-axis in a sequence (ABCABC) (Figures 3b and 4a). Furthermore, all oxygen vertices of VO₆ polyhedra in the cluster are shared with orthophosphate tetrahedra. Thus, tetramers of V-centered octahedra unite via PO₄ groups along the [001] direction into a close-packed framework crystal structure (Figure 3).

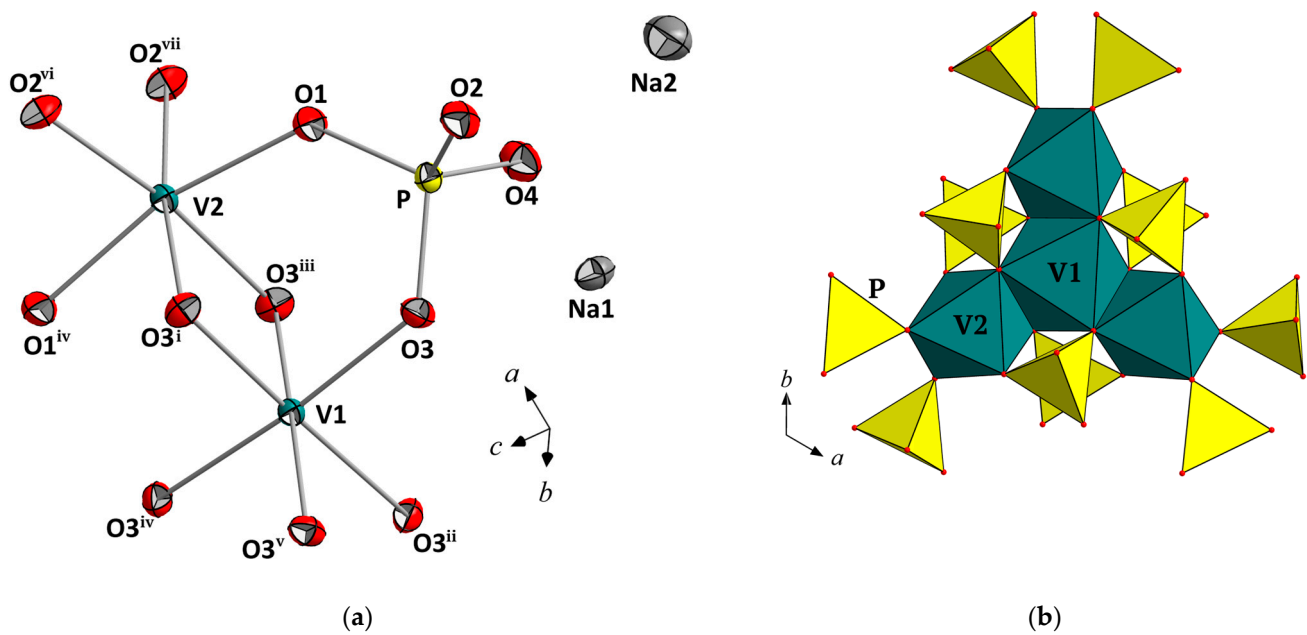


Figure 2. The main building units of the $\text{Na}_7\text{V}_4(\text{PO}_4)_6$ structure. (a) Atoms are shown in ellipsoid mode at a 90% probability level (symmetry operations: (i) $-x + 2/3, -x + y + 1/3, -z + 5/6$; (ii) $-x + y, -x + 1, z$; (iii) $-y + 1, x - y + 1, z$; (iv) $x - y + 2/3, -y + 4/3, -z + 5/6$; (v) $y - 1/3, x + 1/3, -z + 5/6$; (vi) $x + 1/3, x - y + 2/3, z + 1/6$; (vii) $y + 1/3, -x + y + 2/3, -z + 2/3$). (b) The cluster of four vanadium octahedra in surrounding phosphate.

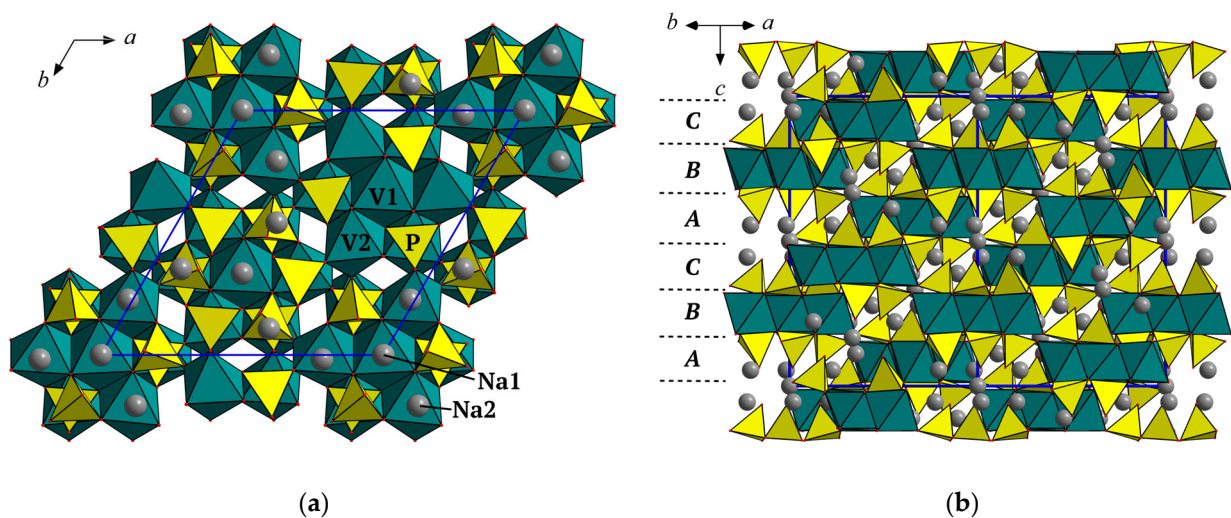


Figure 3. Crystal structure of the $\text{Na}_7\text{V}_4(\text{PO}_4)_6$ projected along (a) the $[0001]$ and (b) the $[11\bar{2}0]$ directions.

The negative charge of the heteropolyhedral anionic framework $[\text{V}_4(\text{PO}_4)_6]^{7-}$ is compensated by Na cations, which occupy two symmetrically different sites in the structure. Regular Na_1O_6 octahedra with C_{3i} symmetry have six identical Na1–O4 distances of 2.362(1) Å (Table 2). The Na_2O_6 octahedron with intrinsic C_1 symmetry is strongly distorted: the Na–O bond lengths range in the interval 2.271(2)–2.640(2) Å with an average value of 2.534 Å. Three additional oxygen atoms are at distances of 2.808(2), 2.877(2), and 3.021(1) Å (Table 2). Sodium polyhedra share faces and edges to form clusters of seven units with a central Na_1O_6 octahedron and Na_2O_6 octahedra multiplied by six due to the $\bar{3}$ inversion axis. Similar to vanadium tetramers, these clusters in a cut layer parallel to the (001) plane are arranged in the densest manner (Figure 4). These layered fragments alternate in the sequence (ABCABC) corresponding to the cubic close-packing (Figure 3).

Along the *c*-axis, sodium heptamers interconnect through common O₄–O₄ edges of Na₂O₆ polyhedra and form a three-periodic cationic framework.

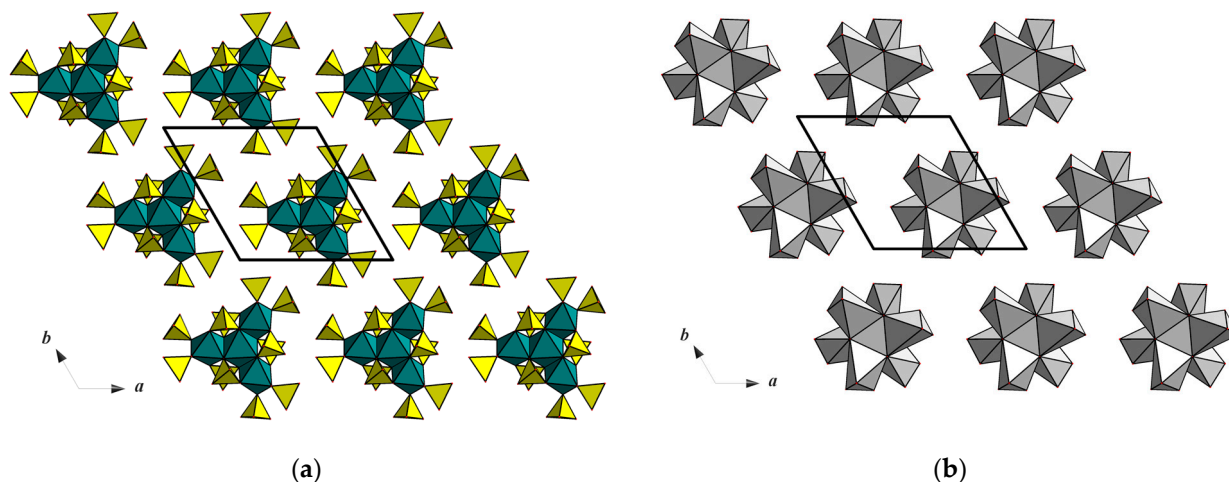


Figure 4. Layered “cut” of the crystal structure of Na₇V₄(PO₄)₆ on the *ab* plane: (a) clusters of four vanadium octahedra surrounded by PO₄-tetrahedra and (b) clusters of sodium octahedra, both arranged according to the close-packing law.

3.2. BVS Calculations and XANES Spectroscopy

The requirement for electroneutrality of the title compound is achieved by including vanadium cations of two valence states, V²⁺ and V³⁺. Close values of V–O distances characterize both polyhedra centered with vanadium (Table 2). Furthermore, the average V–O bond lengths are almost equal: 2.017 and 2.012 Å, which indicates the mixed occupancy of both structural positions by V atoms in the 3+ and 2+ oxidation states. The calculation of bond–valence sums [25,26] confirms the statistical distribution of V³⁺ and V²⁺ ions (Table 3). Based on the theoretical ratio V³⁺/V²⁺ = 3:1, the total vanadium contributions 2.83 and 2.87 are quite close to 2.75, which indicates a mixed valence state of V in both structural sites: Na₇V^{2.75}V^{2.75}₃[PO₄]₆.

Table 3. Bond–valence data ¹.

	V ₁	V ₂	P	Na ₁	Na ₂ ²	Σ
O ₁		0.510 × ₂ ↓	1.189		0.134, 0.075, 0.049	1.96
O ₂		0.501 × ₂ ↓	1.215		0.123, 0.107	1.95
O ₃	0.471 × ₆ ↓	0.425 × ₂ ↓	1.135		0.066	2.10
O ₄			1.328	0.189 × ₆ ↓	0.230, 0.123, 0.111	1.98
Σ	2.83	2.87	4.87	1.13	1.02	

¹ Symbols ×₂↓ and ×₆↓ mark a multiplication of the corresponding contribution along the column due to the symmetry; ² Contributions from all nine neighboring O atoms were taken into account.

In order to determine the formal oxidation state of the absorbing atom (V), the analysis of the shape and position of the XANES spectrum could be used [27–30]. We applied the procedure described in [31]. The oxidation state of vanadium atoms in the sample under study was determined by interpolating the edge position shift. We considered that the position of the edge jump is the energy at which the normalized absorption equals 0.5. Therefore, the spectrum shift at the level of half the absorption jump is assumed to be proportional to the formal oxidation state of the metal (V). The experimental XANES spectra are shown in Figure 5. The spectra of compounds VSO₄·6H₂O and V₂(SO₄)₃ [32] were used as standards because of the same octahedral coordination of vanadium atoms as in the Na₇V₄(PO₄)₆ phase. Thus, it was determined that the formal oxidation state of the

metal is 2.57, which qualitatively confirms the assumption that there are vanadium atoms with two oxidation states: 3+ and 2+.

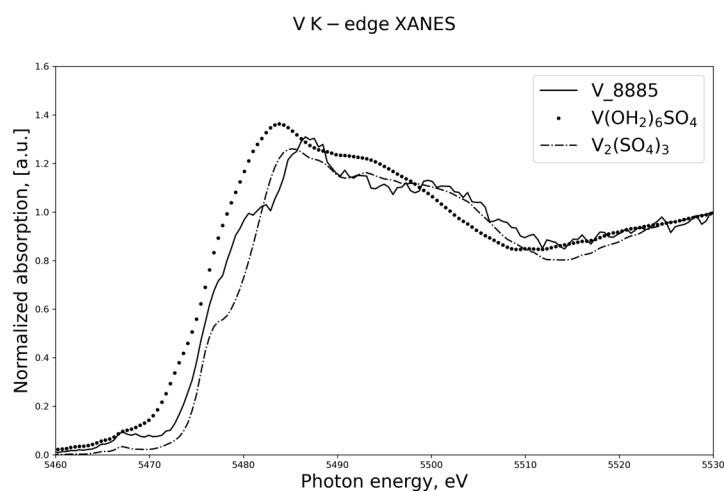


Figure 5. XANES data for the V K-edge of $\text{Na}_7\text{V}_4(\text{PO}_4)_6$ (signed as V_8885) with overlaid spectra of $\text{VSO}_4 \cdot 6\text{H}_2\text{O}$ and $\text{V}_2(\text{SO}_4)_3$.

3.3. The Comparative Crystal Chemistry of $\text{Na}_7\text{V}_4(\text{PO}_4)_6$ and the Database Survey of V^{2+} -Containing Oxosalts

As mentioned in the Introduction, the titled vanadium phosphate is a member of the family of compounds with the general formula $(\text{X})_6(\text{M1})(\text{M2})(\text{M3})_3(\text{TO}_4)_6$, which includes the fumarole mineral yurmarinite, $\text{Na}_7(\text{Fe}^{3+}, \text{Mg}, \text{Cu})_4(\text{AsO}_4)_6$ [5] and synthetic iron (II, III) phosphate $\text{Na}_7\text{Fe}_4(\text{PO}_4)_6$ [6]. In these two phases, the valence state of the Fe atoms was confirmed by Mössbauer or Raman spectroscopy. Table 4 shows the cation–anion distances for the transition-metal octahedral sites M2 (Wyckoff site 6a, site symmetry 32) and M3 (Wyckoff site 18e, site symmetry 2) populated by V or Fe. The close average values of the M–O bond lengths in the M_2O_6 and M_3O_6 octahedra, equal to 2.02 Å and 2.01 Å, indicate the mixed occupancy of the V positions in the $\text{Na}_7\text{V}_4(\text{PO}_4)_6$ crystal structure. In addition, the M–O bond lengths are close enough in the Fe- and V-bearing phases. This similarity results from the close values of the cationic radii of these transition metals in the same valence states and in the same octahedral coordination ($r\text{V}^{2+} = 0.79$ Å, $r\text{Fe}^{2+} = 0.78$ Å; $r\text{V}^{3+} = 0.64$ Å, $r\text{Fe}^{3+} = 0.63$ Å [33]). The V ionic radii are slightly smaller than those of iron; accordingly, the unit-cell parameters and volume of $\text{Na}_7\text{V}_4(\text{PO}_4)_6$ are also smaller than those of $\text{Na}_7\text{Fe}_4(\text{PO}_4)_6$. The unit-cell parameters of yurmarinite are the largest due to the larger size of arsenate tetrahedra compared to phosphate groups.

Table 4. Unit-cell parameters (Å), volumes (Å³), and interatomic distances (Å) for V/Fe octahedra in $\text{Na}_7\text{V}_4(\text{PO}_4)_6$, $\text{Na}_7\text{Fe}_4(\text{PO}_4)_6$, and yurmarinite, $\text{Na}_7(\text{Fe}^{3+}, \text{Mg}, \text{Cu})_4(\text{AsO}_4)_6$ crystal structures (space group $R\bar{3}c$, $Z = 6$).

	$\text{Na}_7\text{V}_4(\text{PO}_4)_6$	$\text{Na}_7\text{Fe}_4(\text{PO}_4)_6$	Yurmarinite, $\text{Na}_7(\text{Fe}^{3+}, \text{Mg}, \text{Cu})_4(\text{AsO}_4)_6$
<i>a</i> (<i>b</i>)	13.3463(19)	13.392(2)	13.7444(2)
<i>c</i>	17.809(4)	17.858(3)	18.3077(3)
<i>V</i>	2747.2(10)	2773.7(8)	2995.14(8)
M2–O ₃ × 6	2.0173(13)	2.063(2)	1.9429(18)
<M2–O>	2.02	2.06	1.94
M3–O ₁ × 2	1.9877(13)	1.974(2)	1.991(2)
M3–O ₂ × 2	1.9942(14)	1.997(2)	2.0142(19)
M3–O ₃ × 2	2.0548(13)	2.085(1)	2.1170(19)
<M3–O>	2.01	2.02	2.04

Table 5 lists all V²⁺-bearing oxosalts with known crystal structures collected in the ICSD database. Five listed phases include exceptionally V²⁺ compounds, while seven of the other listed compounds contain both V²⁺ and V³⁺ cations. In all crystal structures, V occupies octahedral positions.

Table 5. Synthetic and natural oxygen-containing inorganic compounds with divalent vanadium.

Compound/ Mineral	Space Group, Z, ρ , mg/m ³	Unit-Cell Para-Meters, <i>a</i> , <i>b</i> , <i>c</i> , Å and Angles, °	R	Range of V–O Distances in Octahedra, Å	Synthesis Technique/Natural Genesis	Ref.
(NH ₄) ₂ V(SO ₄) ₂ ·6H ₂ O NH ₄ ,V- analogue of picromerite and Tutton's salt	<i>P</i> 2 ₁ / <i>a</i> 2, 1.80	<i>a</i> = 9.42(3) <i>b</i> = 12.76(3) <i>c</i> = 6.22(2) β = 107.2(2)	0.08	2.118–2.164 <2.15>	Modification of Kranz method to obtain VOSO ₄ , its further cooling and electrolytic reduction in H ₂ SO ₄ solution, then the addition of pyrogallol and recrystallization in N ₂ atmosphere.	[34]
V(H ₂ O) ₆ SO ₄ V-analogue of hexahydrate	<i>C</i> 2/ <i>c</i> 8, 1.91	<i>a</i> = 10.081(3) <i>b</i> = 7.286(2) <i>c</i> = 24.445(7) β = 98.78(2)	0.039	2.123–2.136 <2.13> 2.120–2.150 <2.13>	Modification of the Kranz method. Electrochemical reduction of VOSO ₄ ·2H ₂ O in the solution of H ₂ SO ₄ under N ₂ or Ag atmosphere followed by adding ethanol on cooling.	[35]
V(H ₂ O) ₆ SO ₄ ·H ₂ O	<i>P</i> 2 ₁ / <i>c</i> 4, 1.86	<i>a</i> = 14.130(3) <i>b</i> = 6.501(1) <i>c</i> = 11.017(2) β = 105.64(2)	0.029	2.102–2.137 <2.12> 2.119–2.150 <2.13>	Recrystallization of VSO ₄ ·6H ₂ O precursor in the solution of H ₂ SO ₄ in N ₂ atmosphere with the addition of ethanol and cooling.	[36]
Li ₂ VPO ₄ F closely related to tavorite str. type	<i>C</i> 2/ <i>c</i> 4, 3.17	<i>a</i> = 7.2255(1) <i>b</i> = 7.9450(1) <i>c</i> = 7.3075(1) β = 116.771(1)	0.049 *	2.119–2.139 <2.13>	Solid-state synthesis of LiV(PO ₄)F at 750 °C in an Ar atmosphere, followed by Li-intercalation with LiAlH ₄ in tetrahydrofuran under Ar.	[37]
Li ₂ V ₂ (SO ₄) ₃ derivative of NASICON str. type	<i>C</i> 2/ <i>c</i> 4, 3.01	<i>a</i> = 13.0582(5) <i>b</i> = 8.6526(4) <i>c</i> = 8.72447(4) β = 115.443(2)	0.042 *	2.073–2.230 <2.14>	Electrochemical Li-intercalation in V ₂ (SO ₄) ₃ with <i>n</i> -butyllithium C ₄ H ₉ Li in a vacuum.	[38]
V ^{2+,3+} ₂ OPO ₄ (high-T modif.)	<i>I</i> 4 ₁ / <i>amd</i> 4, 3.97	<i>a</i> = 5.362(5) <i>c</i> = 12.378(9)	0.044	2.047–2.074 <2.06>	Reduction of VPO ₄ by metallic V at 500 °C and 900 °C via chemical vapor transport in I ₂ .	[39]

Table 5. Cont.

Compound/ Mineral	Space Group, Z, ρ , mg/m ³	Unit-Cell Para-Meters, <i>a</i> , <i>b</i> , <i>c</i> , Å and Angles, °	R	Range of V–O Distances in Octahedra, Å	Synthesis Technique/Natural Genesis	Ref.
V ^{2+,3+} ₂ OPO ₄ (low- temperature modification)	C2/c 4, 3.98	<i>a</i> = 7.56825(7) <i>b</i> = 7.60013(7) <i>c</i> = 7.21794(6) β = 121.2751(5)	0.074 *	2.054–2.123 <2.09> 1.972–2.079 <2.03>	β -VOPO ₄ preparation at 600 °C in flowing O ₂ ; further solid-state synthesis at 1000 °C with metallic V in a vacuum.	[40]
SrV ^{3+,2+} ₁₀ O ₁₅ **	Ccmb 4, 5.20	<i>a</i> = 9.915 <i>b</i> = 11.574 <i>c</i> = 9.324	0.08	1.948–2.192 <2.01> 1.950–2.148 <2.05> 1.965–2.195 <2.04>	Solid-state synthesis at 1900 °C in H ₂ atmosphere	[41]
Al(V ^{2+,3+}) ₂ O ₄ (frustrated spinel)	R $\bar{3}m$ 2, 4.65	<i>a</i> = 5.7613(2) <i>c</i> = 28.6876(10)	0.011 *	2.052–2.063 <2.06> 2.007	Solid-state synthesis with metallic Al at 1150 °C for 150 h in vacuum, phase transition at 427 °C	[42,43]
Al(V ^{2+,3+}) ₂ O ₄ (inverse spinel)	Fd $\bar{3}m$ 8, 4.66	<i>a</i> = 8.1546(6)	No data	2.040	Solid-state synthesis with metallic V at 900 °C in a vacuum	[44,45]
Dellagiustaitite, Al(V ^{2+,3+}) ₂ O ₄ (inverse spinel)	Fd $\bar{3}m$ 8, 4.62	<i>a</i> = 8.1950(1)	0.014	2.045	High redox conditions, probable crystallization from high-temperature melts of volcanic magma	[4]
NaV ^{3+,2+} ₃ (PO ₄) ₃	Imma 4, 3.42	<i>a</i> = 10.488(2) <i>b</i> = 13.213(3) <i>c</i> = 6.455(7)	0.056	1.959–2.062 <1.99> 2.042–2.086 <2.06>	Step-wise solid-state synthesis at 900 °C in a vacuum	[46]
Na ₇ V ^{3+,2+} ₄ (PO ₄) ₆ V, P-analogue of yurmarinite	R $\bar{3}c$ 6, 3.39	<i>a</i> = 13.3463(19) <i>c</i> = 17.809(4)	0.023	2.017 1.988–2.055 <2.01>	High-temperature hydrothermal synthesis at 450 °C with Na ₃ C ₆ H ₅ O ₇ redox agent	This work

* Based on power data, including synchrotron and neutron radiation sources; ** Isostructural with BaV^{3+,2+}₁₀O₁₅ [47].

Urusov and Serezhkin [48] showed that the V²⁺ and V³⁺ cations form regular octahedra with average V–O bond lengths equal to 2.13 and 2.01 Å. Similarly, the data from Table 5 show that the average V–O distances range slightly from 2.12 Å to 2.18 Å for V²⁺-centered octahedra and from 2.01 Å to 2.09 Å for polyhedra isomorphically occupied by V²⁺ and V³⁺ cations. It is consistent with the smaller ionic radius of V³⁺ (0.64 Å) compared to V²⁺ (0.79 Å) [33]. For the title Na₇V₄(PO₄)₆ compound, with a mixed valence state of vanadium, the average <V–O> distance of 2.02 Å lies in the lower part of the region for compounds with V^{2+,3+}-centered polyhedra.

Although the first inorganic oxide of divalent vanadium was synthesized more than a hundred years ago, the number of compounds containing V²⁺ ions in “formula” amounts is still small. The main reason for the small number of V²⁺ oxosalts is their high instability in the air, which significantly complicates the synthesis and preparation of precursors [49]. Three methods for synthesizing vanadium oxosalts are commonly used, and all require an inert atmosphere and redox reagents. First, Kranz suggested a synthesis by a stepwise reduction of V₂O₅ by electrolysis [50]. This method was modified by Shlenck’s techniques and became the basis for the synthesizing of V²⁺ hydrate sulfates (Table 5). One major feature of these compounds is the presence of water molecules in V²⁺ octahedral coordination. Consequently, all the structures possess low density equal to 1.8–1.9 Mg/m³.

The second method, the Li-intercalation, was used to obtain $\text{Li}_2\text{V}^{2+}(\text{PO}_4)\text{F}$ related to tavorite and $\text{Li}_2\text{V}^{2+}_2(\text{SO}_4)_3$ with the NASICON-derived structure. Later, by the third method, heterovalent ($\text{V}^{2+,3+}$) compounds were synthesized using a high-temperature solid-state reaction. As a result, $\alpha\text{-CrPO}_4$ -type $\text{NaV}^{3+,2+}_3(\text{PO}_4)_3$, two polymorphic oxophosphates $\text{V}^{2+,3+}_2\text{OPO}_4$, two isostructural oxides $\text{SrV}^{3+,2+}_{10}\text{O}_{15}$ and $\text{BaV}^{3+,2+}_{10}\text{O}_{15}$, and two spinel polymorphs $\text{Al}(\text{V}^{2+,3+})_2\text{O}_4$ were obtained by the third method. Interestingly, both spinels and exceptionally Sr or Ba vanadium oxides feature structures based on the hexagonal close-packing and thus have a high density of 4.6–5.2 Mg/m^3 . Noteworthy, the same inverse spinel, $\text{Al}(\text{V}^{2+},\text{V}^{3+})_2\text{O}_4$, called dellagiustaite, was recently found in nature and presented a unique mineral with V^{2+} cations as an essential element in its composition. However, it is difficult to establish the genesis of dellagiustaite due to the lack of information about the exact location of the outcrop and related rocks [4]. However, exclusively reducing conditions are necessary for mineral formation because it is associated with almost pure vanadium alloys.

We successfully obtained heterovalent V(II, III) phosphate under hydrothermal conditions. In solution under normal conditions, vanadium dissolves and exists as the V^{2+} cation under acidic and redox conditions exclusively, i.e., at $\text{pH} = -2$ – 2 and $\text{Eh} = -1$ – 0 V, according to the thermodynamic data of the Gibbs free energy for vanadium (see, for example, [51]). The high solubility of phosphoric acid and the use of $\text{Na}_3\text{C}_6\text{H}_5\text{O}_7$ as a redox agent allowed us to obtain two sodium vanadium phosphates: NASICON $\text{Na}_3\text{V}^{3+}_2(\text{PO}_4)_3$ with the kosnarite structure type and $\text{Na}_7\text{V}^{3+,2+}_4(\text{PO}_4)_6$ with the yurmarinite structure type. Therefore, we can assume that the "metastable" $\text{Na}_7\text{V}_4(\text{PO}_4)_6$ was formed as a primary phase at a higher temperature and a lower pH value. It is likely that the more stable compound $\text{Na}_3\text{V}_2(\text{PO}_4)_3$ was formed subsequently upon smooth cooling of the autoclave.

3.4. Topological Analysis of Ion Conductivity of $\text{Na}_7\text{V}_4(\text{PO}_4)_6$

Vanadium provides an excellent opportunity to exchange more than one electron per transition metal, resulting in a high theoretical energy density [52]. In addition, the presence of many Na^+ ions in the crystal structure can also lead to the possible activation of plenty of redox transitions $\text{V}^{2+}/\text{V}^{3+}/\text{V}^{4+}/\text{V}^{5+}$ during the electrochemical extraction of sodium. Currently, four Na_xV^{3+} phosphates are known to possess electrochemical properties. We obtained one of them, $\text{Na}_3\text{V}_2(\text{PO}_4)_3$, as a byproduct of the synthesis. It is a synthetic variety of mineral kosnarite, $\text{KZr}_2(\text{PO}_4)_3$, whose crystal structure is close to that of the sodium superionic conductor NASICON. $\text{Na}_3\text{V}_2(\text{PO}_4)_3$ exhibits high energy density, thermal and structure stability, ion conductivity, and a high-voltage plateau at 3.4 V [53–56]. Likewise, other Na_xV^{3+} phosphates, namely $\text{Na}_3\text{V}(\text{PO}_4)_2$ [57,58], $\text{Na}_3\text{V}_3(\text{PO}_4)_4$ [59], and $\text{NaV}_3(\text{PO}_4)_3$ [30,46] represent high-voltage cathode/high-performance anode materials for sodium batteries [60]. We emphasize that the $\text{Na}_3\text{V}(\text{PO}_4)_2$ crystal structure is also related to mineral apthitalite; both $\text{Na}_3\text{V}_3(\text{PO}_4)_4$ and $\text{NaV}_3(\text{PO}_4)_3$ crystal structures are closely related to that of $\alpha\text{-CrPO}_4$. To evaluate the electrochemical properties without sufficient substance for experimental measurements, we applied the theoretical calculation of the ionic conductivity of $\text{Na}_7\text{V}_4(\text{PO}_4)_6$.

To find the migration paths of Na^+ cations throughout the framework [61], we used the geometrical–topological approach from the ToposPro package [62]. The method is based on the Voronoi–Dirichlet partition model, which helps to find out the centers of vacancies and channel lines. The Voronoi–Dirichlet partition model is founded on the following basement. The convex Voronoi polyhedra bend around each of the "framework" atoms. This bending results in the forming of voids located most distant from the structure atoms. Linked together, voids form the net, whose periodicity reflects the ion migration path's topology. Remarkably, the net of voids should be infinite—like a chain, a layer, or a framework—to promote conductivity.

The primary geometric parameters for the Voronoi–Dirichlet model are the radius of the spherical domain R_{sd} and the channel radius R_{ch} . In our calculation, the threshold value of R_{sd} is set equal to 1.31 Å, which is 10% lower than the experimental value for "real"

sodium atoms in the structure (1.50 Å and 1.46 Å). It is much smaller than the theoretical average value of 1.54 Å [63] and close to 1.35 Å estimated from the migration maps of Na-ion conductors in recent studies [64,65]. The threshold value of R_{ch} was asserted to be 2.0 Å following [64]. Theoretically, the structural channel is assumed accessible for ion flotation if the sum of the radii of the mobile ion (Na) and the framework atom (O) exceeds the channel radius R_{ch} by 10–15%. In contrast with the theoretical preposition, the topological analysis shows the absence of migration paths for Na⁺ cations, even though the lowest values of the threshold parameters were taken. Small structural voids with a radius of 1.31 Å to 1.57 Å do not connect with each other in the crystal structure of Na₇V₄(PO₄)₆ and therefore do not form infinite channels large enough for Na⁺ passing.

4. Conclusions

Under high-temperature (450 °C) hydrothermal conditions, we successfully synthesized a new phase Na₇V₄(PO₄)₆, a V^{3+,2+} analogue of the fumarole mineral yurmarinite. We showed that the crystal structure of Na₇V₄(PO₄)₆ is based on densely packed layers of vanadium or sodium clusters, which alternate in the ABCABC sequence, and link by [PO₄] tetrahedra. Besides the new compound Na₇V₄(PO₄)₆, the research revealed only twelve oxosalts with V²⁺ or isomorphic V²⁺/V³⁺ cations, including the unique divalent vanadium mineral dellagiustaite. Our study presents the first case of hydrothermally synthesized Na₇V^{3+,2+}₄(PO₄)₆ crystals in addition to electrolysis, Li-intercalation, and the solid-state method used previously to prepare V²⁺ inorganic compounds. We conducted the X-ray diffraction study, BVS calculations, crystal–chemical comparative analysis of V²⁺-bearing compounds, and XANES measurements of Na₇V₄(PO₄)₆ crystals, which confirmed the presence of V²⁺ ions in it. Furthermore, the disability of Na-ion migration through Na₇V₄(PO₄)₆ was shown by performing the topological analysis of its crystal structure.

Supplementary Materials: The following supporting information can be downloaded at: <https://www.mdpi.com/article/10.3390/min12121517/s1>, Table S1: Atomic coordinates and equivalent anisotropic displacement parameters for Na₇V₄(PO₄)₆; Figure S1: Calculated pattern for Na₇V₄(PO₄)₆.

Author Contributions: Conceptualization, O.Y.; methodology, G.K., A.V., A.T. and K.L.; validation, O.Y.; investigation, G.K., V.N., O.Y., A.V., O.D., A.T. and K.L.; writing—original draft preparation, V.N. and G.K.; writing—review and editing, O.Y. All authors have read and agreed to the published version of the manuscript.

Funding: This research was funded by a grant from the President of the Russian Federation for young scientists—candidates of science MK-1613.2021.1.5.

Data Availability Statement: Not applicable.

Acknowledgments: We thank V.O. Yapaskurt for the microprobe analysis of the crystals and E.I. Marchenko for helping with the ToposPro tools. We are grateful to O.M. Kiriukhin from the City University of Hong Kong, for checking the English.

Conflicts of Interest: The authors declare no conflict of interest.

References

1. Liu, C.; Eleish, A.; Hystad, G.; Golden, J.J.; Downs, R.T.; Morrison, S.M.; Hummer, D.R.; Ralph, J.P.; Fox, P.; Hazen, R.M. Analysis and visualization of vanadium mineral diversity and distribution. *Am. Miner.* **2018**, *103*, 1080–1086. [CrossRef]
2. Schindler, M.; Hawthorne, F.C.; Baur, W.H. A crystal-chemical approach to the composition and occurrence of vanadium minerals. *Can. Miner.* **2000**, *38*, 1443–1456. [CrossRef]
3. O’Loughlin, E.J.; Boyanov, M.I.; Kemner, K.M. Reduction of Vanadium(V) by Iron(II)-Bearing Minerals. *Minerals* **2021**, *11*, 316. [CrossRef]
4. Cámara, F.; Bindi, L.; Pagano, A.; Pagano, R.; Gain, S.E.; Griffin, W.L. Dellagiustaite: A Novel Natural Spinel Containing V²⁺. *Minerals* **2019**, *9*, 4. [CrossRef]
5. Pekov, I.V.; Zubkova, N.V.; Yapaskurt, V.O.; Belakovskiy, D.I.; Lykova, I.S.; Viggasina, M.F.; Sidorov, E.G.; Pushcharovsky, D.Y. New arsenate minerals from the Arsenatnaya fumarole, Tolbachik volcano, Kamchatka, Russia. I. Yurmarinite, Na₇(Fe³⁺,Mg,Cu)₄(AsO₄)₆. *Miner. Mag.* **2014**, *78*, 905–917. [CrossRef]

6. Lii, K.-H. $\text{Na}_7\text{Fe}_4(\text{PO}_4)_6$: A mixed-valence iron phosphate containing a tetramer of edge-sharing FeO_6 octahedra. *J. Chem. Soc. Dalton Trans.* **1996**, *6*, 819–822. [[CrossRef](#)]
7. Masquelier, C.; d'Yvoire, F.; Collin, G. Crystal structure of $\text{Na}_7\text{Fe}_4(\text{AsO}_4)_6$ and $\alpha\text{-Na}_3\text{Al}_2(\text{AsO}_4)_3$, two sodium ion conductors structurally related to $\text{II-Na}_3\text{Fe}_2(\text{AsO}_4)_3$. *J. Solid State Chem.* **1995**, *118*, 33–42. [[CrossRef](#)]
8. Bourguiba, N.F.; Ouerfelli, N.; Zid, M.F. Crystal Structure, Charge-Distribution and Bond-Valence-Sum Investigations of a Novel Arsenate $\text{Na}_{3.5}\text{Cr}_{1.83}(\text{AsO}_4)_3$. *J. Adv. Chem.* **2014**, *10*, 3160–3170.
9. Bourguiba, N.F.; Guesmi, A.; Ouerfelli, N.; Mazza, D.; Zid, M.F.; Driss, A. Le Nouvel Arséniate $\text{Ag}_{1.60}\text{Na}_{1.40}\text{Al}_2(\text{AsO}_4)_3$: Synthèse, Études Structurale Et Électrique, Simulation Des Chemins De Conduction Ionique. *J. Soc. Chim. Tunis.* **2012**, *14*, 201–211.
10. Gulyaeva, O.A.; Solodovnikova, Z.A.; Solodovnikov, S.F.; Zolotova, E.S.; Mateyshina, Y.G.; Uvarov, N.F. Triple molybdates $\text{K}_{3-x}\text{Na}_{1+x}\text{M}_4(\text{MoO}_4)_6$ ($\text{M} = \text{Ni}, \text{Mg}, \text{Co}$) and $\text{K}_{3+x}\text{Li}_{1-x}\text{Mg}_4(\text{MoO}_4)_6$ isotopic with $\text{II-Na}_3\text{Fe}_2(\text{AsO}_4)_3$ and yurmarinite: Synthesis, potassium disorder, crystal chemistry and ionic conductivity. *Acta Cryst.* **2020**, *B76*, 913–925.
11. D'Yvoire, F.; Bretey, E.; Collin, G. Crystal structure, non-stoichiometry and conductivity of $\text{II-Na}_3\text{M}_2(\text{AsO}_4)_3$ ($\text{M} = \text{Al}, \text{Ga}, \text{Cr}, \text{Fe}$). *Solid State Ion.* **1988**, *28*, 1259–1264. [[CrossRef](#)]
12. Yakubovich, O.V. Microporous Vanadylphosphates—Perspective Materials for Technological Applications. In *Minerals as Advanced Materials II*; Krivovichev, S., Ed.; Springer: Berlin, Heidelberg, 2011; pp. 239–253.
13. Yakubovich, O.V.; Steele, I.M.; Yakovleva, E.V.; Dimitrova, O.V. One-dimensional decavanadate chains in the crystal structure of $\text{Rb}_4[\text{Na}(\text{H}_2\text{O})_6][\text{HV}_{10}\text{O}_{28}] \cdot 4\text{H}_2\text{O}$. *Acta Cryst.* **2015**, *C71*, 465–473.
14. Yakubovich, O.V.; Kiryukhina, G.V.; Dimitrova, O.V. Crystal chemistry of $\text{KCuMn}_3(\text{VO}_4)_3$ in the context of detailed systematics of the alluaudite family. *Crystallogr. Rep.* **2016**, *61*, 566–575. [[CrossRef](#)]
15. Shvanskaya, L.V.; Yakubovich, O.V.; Krikunova, P.V.; Kiriukhina, G.V.; Ivanova, A.G.; Volkov, A.S.; Dimitrova, O.V.; Borovikova, E.Y.; Volkova, O.S.; Vasiliev, A.N. Nonstoichiometric ellenbergerite-type phosphates: Hydrothermal synthesis, crystal chemistry, and magnetic behavior. *Inorg. Chem.* **2022**, *61*, 4879–4886. [[CrossRef](#)]
16. Zatonvsky, I.V. Nasicon-type $\text{Na}_3\text{V}_2(\text{PO}_4)_3$. *Acta Cryst.* **2010**, *E66*, 112. [[CrossRef](#)]
17. Farrugia, L.J. WinGX and ORTEP for Windows: An update. *J. Appl. Cryst.* **2012**, *45*, 849–854. [[CrossRef](#)]
18. Sheldrick, G.M. SHELXT—Integrated space-group and crystal-structure determination. *Acta Cryst.* **2015**, *A71*, 3–8. [[CrossRef](#)]
19. Sheldrick, G.M. Crystal structure refinement with SHELXL. *Acta Cryst.* **2015**, *C71*, 3–8.
20. Rigaku, O.D. *CrysAlis PRO*; Rigaku Oxford Diffraction Ltd.: Yarnton, Oxfordshire, UK, 2018.
21. Krause, L.; Herbst-Irmer, R.; Sheldrick, G.M.; Stalke, D. Comparison of silver and molybdenum microfocus X-ray sources for single-crystal structure determination. *J. Appl. Cryst.* **2015**, *48*, 3–10. [[CrossRef](#)]
22. Brandenburg, K. *Diamond*; Crystal Impact GbR: Bonn, Germany, 2006.
23. Chernyshov, A.A.; Veligzhanin, A.A.; Zubavichus, Y.V. Structural Materials Science end-station at the Kurchatov Synchrotron Radiation Source: Recent instrumentation upgrades and experimental results. *Nucl. Instrum. Methods Phys. Res.* **2009**, *A603*, 95–98. [[CrossRef](#)]
24. Newville, M. Larch: An analysis package for XAFS and related spectroscopies. *J. Phys. Conf. Ser.* **2013**, *430*, 012007. [[CrossRef](#)]
25. Brown, I.D.; Altermatt, D. Bond-valence parameters obtained from a systematic analysis of the inorganic crystal structure database. *Acta Cryst.* **1985**, *B41*, 244–247. [[CrossRef](#)]
26. Brown, I.D. Recent developments in the methods and applications of the bond valence model. *Chem. Rev.* **2009**, *109*, 6858–6919. [[CrossRef](#)] [[PubMed](#)]
27. Charles, D.S.; Guo, F.; Shan, X.; Kim, S.; Lebens-Higgins, Z.W.; Xu, W.; Su, D.; Piper, L.F.J.; Teng, X. Dual-stage K^+ ion intercalation in V_2O_5 -conductive polymer composites. *J. Mater. Chem.* **2021**, *A9*, 15629–15636. [[CrossRef](#)]
28. Dau, H.; Iuzzolino, L.; Dittmer, J. The tetra-manganese complex of photosystem II during its redox cycle—X-ray absorption results and mechanistic implications. *Biochim. Biophys. Acta Bioenerg.* **2001**, *1503*, 24–39. [[CrossRef](#)] [[PubMed](#)]
29. Lee, J.B.; Chae, O.B.; Chae, S.; Ryu, J.H.; Oh, S.M. Amorphous Vanadium Titanates as a Negative Electrode for Lithium-ion Batteries. *J. Electrochem. Sci. Technol.* **2016**, *7*, 306–315. [[CrossRef](#)]
30. Wang, X.; Hu, P.; Chen, L.; Yao, Y.; Kong, Q.; Cui, G.; Shi, S.; Chen, L. An $\alpha\text{-CrPO}_4$ -type $\text{NaV}_3(\text{PO}_4)_3$ anode for sodium-ion batteries with excellent cycling stability and the exploration of sodium storage behavior. *J. Mater. Chem.* **2017**, *A5*, 3839–3847. [[CrossRef](#)]
31. Gustafsson, J.P. Vanadium geochemistry in the biogeosphere—speciation, solid-solution interactions, and ecotoxicity. *Appl. Geochem.* **2019**, *102*, 1–25. [[CrossRef](#)]
32. Haskel, D.; Islam, Z.; Lang, J.; Kmety, C.; Srajer, G.; Pokhodnya, K.I.; Epstein, A.J.; Miller, J.S. Local structural order in the disordered vanadium tetracyanoethylene room-temperature molecule-based magnet. *Phys. Rev.* **2004**, *B70*, 054422. [[CrossRef](#)]
33. Shannon, R.D. Revised effective ionic radii and systematic studies of interatomic distances in halides and chalcogenides. *Acta Cryst.* **1976**, *B32*, 751–767. [[CrossRef](#)]
34. Montgomery, H.; Morosin, B.; Natt, J.J.; Witkowska, A.T.; Lingafelter, E.C. The crystal structure of Tutton's salts. VI. Vanadium (II), iron (II) and cobalt (II) ammonium sulfate hexahydrates. *Acta Cryst.* **1967**, *22*, 775–780. [[CrossRef](#)]
35. Cotton, F.A.; Falvello, L.R.; Llusar, R.; Libby, E.; Murillo, C.A.; Schwotzer, W. Synthesis and characterization of four vanadium (II) compounds, including vanadium (II) sulfate hexahydrate and vanadium (II) saccharinates. *Inorg. Chem.* **1986**, *25*, 3423–3428. [[CrossRef](#)]

36. Cotton, F.A.; Falvello, L.R.; Murillo, C.A.; Pascual, I.; Schultz, A.J.; Tomás, M. Neutron and X-ray Structural Characterization of the Hexaaquavanadium (II) Compound $VSO_4 \cdot 7H_2O$. *Inorg. Chem.* **1994**, *33*, 5391–5395. [[CrossRef](#)]
37. Ellis, B.L.; Ramesh, T.N.; Davis, L.J.M.; Goward, G.R.; Nazar, L.F. Structure and electrochemistry of two-electron redox couples in lithium metal fluorophosphates based on theavorite structure. *Chem. Mater.* **2011**, *23*, 5138–5148. [[CrossRef](#)]
38. Vaughan, G.B.M.; Gaubicher, J.; Le Mercier, T.; Angenault, J.; Quarton, M.; Chabre, Y. Crystal structure of the end product of electrochemical lithium intercalation in $V_2(SO_4)_3$. *Mater. Chem.* **1999**, *9*, 2809–2812. [[CrossRef](#)]
39. Glaum, R.; Gruehn, R. Beiträge zum thermischen Verhalten von wasserfreien Phosphaten. Synthese, Kristallstruktur und magnetisches Verhalten von V_2PO_5 . *Z. Kristallogr. Cryst. Mater.* **1989**, *186*, 91–93.
40. Pachoud, E.; Cumby, J.; Lithgow, C.T.; Attfield, J.P. Charge order and negative thermal expansion in V_2OPO_4 . *J. Am. Chem. Soc.* **2018**, *140*, 636–641. [[CrossRef](#)]
41. De Beaulieu, D.C.; Müller-Buschbaum, H. Gemischtvalente Oxovanadate. II. Synthese und Kristallstruktur von $SrV_{10}O_{15}$. *Z. Anorg. Allg. Chem.* **1981**, *472*, 33–37. [[CrossRef](#)]
42. Matsuno, K.I.; Katsufuji, T.; Mori, S.; Moritomo, Y.; Machida, A.; Nishibori, E.; Takata, M.; Sakata, M.; Yamamoto, N.; Takagi, H. Orbital Order and Phase Transitions in Vanadium Spinels. *J. Phys. Soc. Japan* **2001**, *70*, 1456–1459. [[CrossRef](#)]
43. Horibe, Y.; Shingu, M.; Kurushima, K.; Ishibashi, H.; Ikeda, N.; Kato, K.; Motome, Y.; Furukawa, N.; Mori, S.; Katsufuji, T. Spontaneous formation of vanadium “molecules” in a geometrically frustrated crystal: AlV_2O_4 . *Phys. Rev. Lett.* **2006**, *96*, 086406. [[CrossRef](#)]
44. Reuter, B.; Aust, R.; Colsmann, G.; Neuwald, C. Darstellung und Eigenschaften Vanadium (II)-haltiger und damit n-leitender Vanadium (III)-Spinelle. *Z. Anorg. Allg. Chem.* **1983**, *500*, 188–198. [[CrossRef](#)]
45. Kalavathi, S.; Raju, S.V.; Williams, Q.; Sahu, P.C.; Sastry, V.S.; Sahu, H.K. Pressure-induced frustration in charge ordered spinel AlV_2O_4 . *J. Phys. Cond. Matter* **2013**, *25*, 292201. [[CrossRef](#)] [[PubMed](#)]
46. Kinomura, N.; Matsui, N.; Kumada, N.; Muto, F. Synthesis and crystal structure of $NaV_3P_3O_{12}$: A stuffed structure of α - $CrPO_4$. *J. Solid State Chem.* **1989**, *79*, 232–237. [[CrossRef](#)]
47. Liu, G.; Greedan, J.E. Structure and Magnetism in $AB_{10}O_{15+x}$ ($A = Sr, Ba; B = V, Cr; x = 0, \sim 1$): Evidence for Geometric Frustration. *J. Solid State Chem.* **1996**, *122*, 416–427. [[CrossRef](#)]
48. Urusov, V.S.; Serezhkin, V.N. Distortion of $V^{2+}O_n$ coordination polyhedra and parameters of the bond valence model for VO bonds in inorganic crystals. *Crystallogr. Rep.* **2009**, *54*, 190–194. [[CrossRef](#)]
49. Cotton, F.A.; Daniels, L.M.; Montero, M.L.; Murillo, C.A. Preparation of vanadium (II) compounds. Structures of a carboxylate and a 3-pyridinesulphonate compound. *Polyhedron* **1992**, *11*, 2767–2774. [[CrossRef](#)]
50. Kranz, M.; Goldberg, D.E.; Ribner, A. Vanadium (II) Sulfate. *Inorg. Synth.* **1963**, *7*, 94–96.
51. Li, W.; Niu, Z.; Zhu, X. Recovery of iron by jarosite crystallization and separation of vanadium by solvent extraction with extractant 7101 from titanium white waste liquid (TWWL). *Water Sci. Technol.* **2021**, *83*, 2025–2037. [[CrossRef](#)]
52. Zeng, X.; Peng, J.; Guo, Y.; Zhu, H.; Huang, X. Research progress on $Na_3V_2(PO_4)_3$ cathode material of sodium ion battery. *Front. Chem.* **2020**, *8*, 635. [[CrossRef](#)]
53. Zhang, B.; Ma, K.; Lv, X.; Shi, K.; Wang, Y.; Nian, Z.; Li, Y.; Wang, L.; Dai, L.; He, Z. Recent advances of NASICON- $Na_3V_2(PO_4)_3$ as cathode for sodium-ion batteries: Synthesis, modifications, and perspectives. *J. Alloys Compd.* **2021**, *867*, 159060. [[CrossRef](#)]
54. Zheng, Q.; Yi, H.; Li, X.; Zhang, H. Progress and prospect for NASICON-type $Na_3V_2(PO_4)_3$ for electrochemical energy storage. *J. Energy Chem.* **2018**, *27*, 1597–1617. [[CrossRef](#)]
55. Jian, Z.; Han, W.; Lu, X.; Yang, H.; Hu, Y.-S.; Zhou, J.; Zhou, Z.; Li, J.; Chen, W.; Chen, D.; et al. Superior electrochemical performance and storage mechanism of $Na_3V_2(PO_4)_3$ cathode for room-temperature sodium-ion batteries. *Adv. Energy Mater.* **2013**, *3*, 156–160. [[CrossRef](#)]
56. Saravanan, K.; Mason, C.W.; Rudola, A.; Wong, K.H.; Balaya, P. The first report on excellent cycling stability and superior rate capability of $Na_3V_2(PO_4)_3$ for sodium ion batteries. *Adv. Energy Mater.* **2013**, *3*, 444–450. [[CrossRef](#)]
57. Kovrugin, V.M.; David, R.; Chotard, J.N.; Recham, N.; Masquelier, C. A high voltage cathode material for sodium batteries: $Na_3V(PO_4)_2$. *Inorg. Chem.* **2018**, *57*, 8760–8768. [[CrossRef](#)] [[PubMed](#)]
58. Kim, J.; Yoon, G.; Kim, H.; Park, Y.U.; Kang, K. $Na_3V(PO_4)_2$: A new layered-type cathode material with high water stability and power capability for Na-ion batteries. *Chem. Mater.* **2018**, *30*, 3683–3689. [[CrossRef](#)]
59. Liu, R.; Liu, H.; Sheng, T.; Zheng, S.; Zhong, G.; Zheng, G.; Liang, Z.; Ortiz, G.F.; Zhao, W.; Mi, J.; et al. Novel 3.9 V Layered $Na_3V_3(PO_4)_4$ Cathode Material for Sodium Ion Batteries. *ACS Appl. Energy Mater.* **2018**, *1*, 3603–3606. [[CrossRef](#)]
60. Ke, L.; Dong, J.; Lin, B.; Yu, T.; Wang, H.; Zhang, S.; Deng, C. A $NaV_3(PO_4)_3@C$ hierarchical nanofiber in high alignment: Exploring a novel high-performance anode for aqueous rechargeable sodium batteries. *Nanoscale* **2017**, *9*, 4183–4190. [[CrossRef](#)]
61. Blatov, V.A.; Shevchenko, A.P. Analysis of voids in crystal structures: The methods of “dual” crystal chemistry. *Acta Cryst.* **2003**, *A59*, 34–44. [[CrossRef](#)]
62. Blatov, V.A.; Shevchenko, A.P.; Proserpio, D.M. Applied topological analysis of crystal structures with the program package ToposPro. *Cryst. Growth Des.* **2014**, *14*, 3576–3586. [[CrossRef](#)]
63. Blatov, V.A. Voronoi–dirichlet polyhedra in crystal chemistry: Theory and applications. *Crystallogr. Rev.* **2004**, *10*, 249–318. [[CrossRef](#)]

-
64. Fedotov, S.S.; Kabanova, N.A.; Kabanov, A.A.; Blatov, V.A.; Khasanova, N.R.; Antipov, E.V. Crystallochemical tools in the search for cathode materials of rechargeable Na-ion batteries and analysis of their transport properties. *Solid State Ion.* **2018**, *314*, 129–140. [[CrossRef](#)]
 65. Meutzner, F.; Münchgesang, W.; Leisegang, T.; Schmid, R.; Zschornak, M.; Ureña de Vivanco, M.; Shevchenko, A.P.; Blatov, V.A.; Meyer, D.C. Identification of solid oxygen-containing Na-electrolytes: An assessment based on crystallographic and economic parameters. *Cryst. Res. Technol.* **2017**, *52*, 1600223. [[CrossRef](#)]